Conditions governing localized high-latitude dayside aurora

H. Korth and B. J. Anderson
Applied Physics Laboratory, Johns Hopkins University, Laurel, Maryland, USA

H. U. Frey, T. J. Immel, and S. B. Mende
Space Sciences Laboratory, University of California, Berkeley, Berkeley, California, USA

Received 23 October 2003; revised 30 December 2003; accepted 13 January 2004; published 24 February 2004.

[1] In a recent study of IMAGE FUV data, *Frey et al.* [2003] examined cases of high-latitude dayside aurora (HiLDA) caused by precipitating electrons predominantly during northward IMF with a strongly positive IMF B_y component. To determine the conditions that control these auroral emissions, we examine field-aligned currents observed by the Iridium constellation for 25 events of prolonged steady IMF orientation with both B_z and B_y positive. We find that localized FACs are sustained under all observed solar wind conditions, but that the occurrence of HiLDA is generally restricted to solar wind proton densities below 4 cm^{-3} and peak current densities higher than 0.7 $\mu A/m^2$. That the solar wind density orders the occurrence of the auroral emissions indicates that magnetosheath plasma has ready access to the field lines carrying the upward current. Assuming that the magnetosheath plasma density and temperature govern the high-altitude conditions on these field lines, we find that the intensity of the HiLDA emissions correlates with an estimate for the particle precipitation energy density based on the Knight relation, using the measured current density and the magnetosheath temperature and density. *INDEX TERMS:* 2407 Ionosphere: Auroral ionosphere (2704); 2411 Ionosphere: Electric fields (2712); 2409 Ionosphere: Current systems (2708); 2431 Ionosphere: Ionosphere/magnetosphere interactions (2736). **Citation:** Korth, H., B. J. Anderson, H. U. Frey, T. J. Immel, and S. B. Mende (2004), Conditions governing localized high-latitude dayside aurora, *Geophys. Res. Lett.*, *31*, L04806, doi:10.1029/2003GL018911.

1. Introduction

[2] Highly localized auroral emissions have been observed in the dayside ionosphere poleward of the auroral oval predominantly during intervals of northward interplanetary magnetic field (IMF) with a strong IMF B_y positive component [*Frey et al.*, 2003]. These high-latitude dayside aurora (HiLDA) emissions can persist over a period of several hours and do not exhibit any significant proton contributions. Analysis of simultaneous FAST observations by *Frey et al.* [2003] showed that HiLDA appears at the foot point of an upward field-aligned current (FAC) leg, located in the center of a clockwise convection cell that is driven by high-latitude duskside reconnection. While these authors identified a strongly positive IMF B_y-component and a low solar wind density as key requirements for the occurrence of HiLDA events, the correlation with the magnitudes of the solar wind densities and field-aligned current densities have not been systematically examined.

[3] The purpose of this study is to characterize the conditions controlling this type of auroral emission. We restrict the analysis to intervals of positive IMF B_y with IMF clock angles between +60° and +90°, which have been shown to favor HiLDA events. We then survey the FACs observed during these periods to determine whether HiLDA always occurs when there are localized upward FACs for $B_y > 0$, and, if not, under what conditions they do occur. The FAC distributions used in this study are obtained from the Iridium constellation, which consists of ~70 satellites distributed over six equally-spaced orbit planes. The satellites are in 780-km altitude, circular polar orbits, which is ideal for monitoring global Birkeland currents [*Anderson et al.*, 2000]. The auroral images associated with the FACs are obtained from the Wideband Imaging Camera (WIC) [*Mende et al.*, 2000a] of the Far-Ultraviolet (FUV) instrument [*Mende et al.*, 2000b] aboard the IMAGE spacecraft. The IMAGE satellite is in an elliptical polar orbit with an apogee altitude of 7.2 R_E and employs a variety of imaging techniques to provide comprehensive global images of plasma populations in the inner magnetosphere [*Burch*, 2000]. The WIC instrument is sensitive to wavelengths between 140 nm and 190 nm.

2. Methodology

[4] The observation of magnetic main-field perturbations by Iridium engineering magnetometers allows the generation of global maps of field-aligned currents by spherical harmonic analysis, as described by *Anderson et al.* [2000] and *Waters et al.* [2001]. Because the sampling interval of each satellite is limited to ~200 s, one hour of data accumulation is required in order to resolve FACs associated with HiLDA emissions, which show a latitudinal extent of ~2°. We therefore restrict attention to intervals for which the IMF is stable in direction. The criteria for the event selection are: (1) that the deviation of the IMF orientation from the average direction be less than ±25° for a time period at least three hours in duration in order to ensure constant IMF forcing; (2) that the average IMF magnitude be at least 5 nT in order to ensure that the FACs are reasonably strong; and (3) that the IMF cone angle be between 45° and 135° to ensure quasi-perpendicular conditions at the bow shock in order to minimize time variations in magnetospheric forcing due to shock dynamics. No additional criteria for the stability of the IMF magnitude

0094-8276/04/2003GL018911$05.00

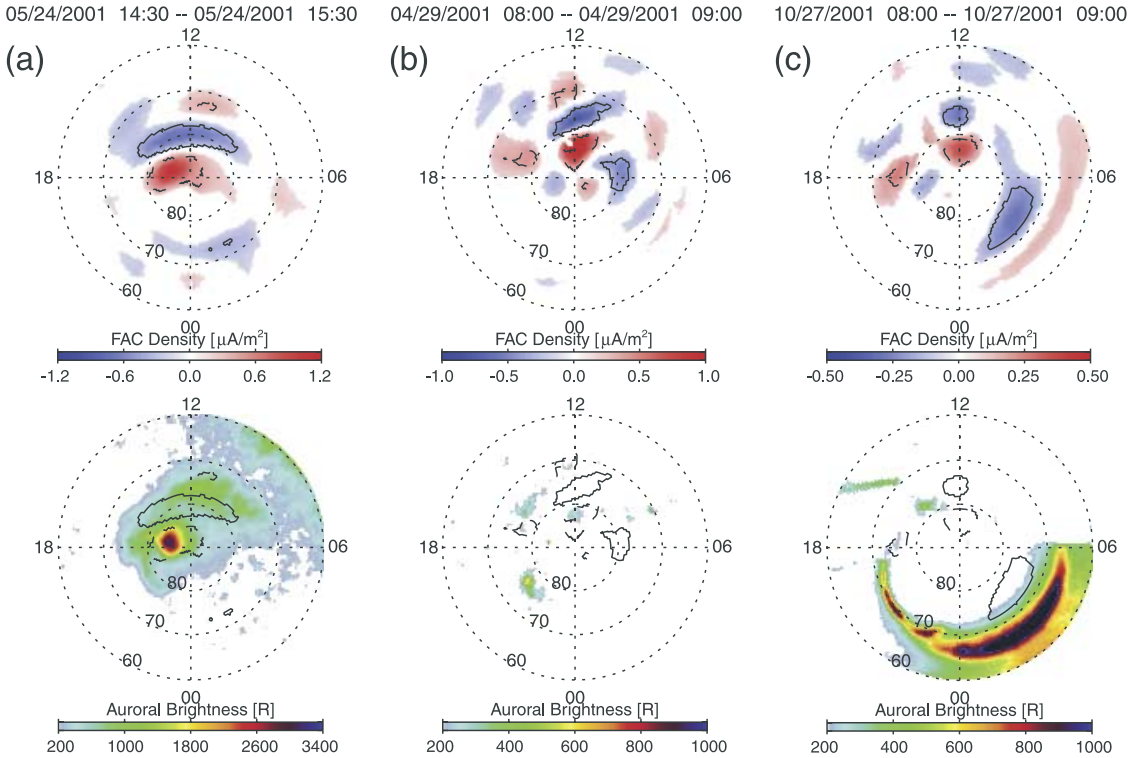

Figure 1. Comparison of Iridium FACs (top row) and IMAGE FUV auroral emissions (bottom row) for three 1-hour intervals on (a) May 24, 2001, (b) April 29, 2001, and (c) October 27, 2001. Only FACs above the 1σ confidence level are shown, where red and blue colors represent upward and downward FACs, respectively. The 2σ confidence level is indicated by contours, which are also overlayed on the FUV images.

are imposed, since the magnitude is generally less variable than the IMF direction, and during these intervals the magnitude typically varies by less than 1 nT.

[5] The solar wind conditions are determined from Level 2 data of the magnetometer (MAG) and Solar Wind Electron Proton Alpha Monitor (SWEPAM) [*Smith et al.*, 1998; *McComas et al.*, 1998] aboard the ACE spacecraft, which is a solar wind monitor located at the first Lagrangian point, L1. By selecting only periods of stable IMF lasting three hours or longer we also ensure that uncertainties in the delay time from the L1 point to Earth are negligible compared to the total length of the stable IMF interval. We therefore use simple advection from ACE to Earth in estimating the IMF and solar wind conditions being imposed on the magnetosphere at the time of the Iridium observations.

[6] The time period selected for this study includes September, 2000, through December, 2001. During this interval there are 56 stable IMF periods of which 25 show high-latitude dayside FACs above the 1σ confidence level and simultaneous viewing of the northern polar cap region by IMAGE FUV. The 1σ confidence level is thereby determined from the departure of the spherical harmonic fit from the magnetic field observations, the spatial distribution of the data points, and the latitude and longitude order used in the spherical harmonic analysis. The 25 intervals include 5 HiLDA events from the *Frey et al.* [2003] study. The remaining 8 intervals of their study are not included because either the interval does not meet the IMF stability requirements, or the IMF clock angle is outside the range considered in this study, or the Iridium FACs are below the 1σ confidence level.

3. Results

[7] Figure 1 shows the Iridium FAC maps together with the IMAGE FUV observations during three stable IMF periods on May 24, 2001, April 29, 2001, and October 27, 2001, hereinafter referred to as events 1, 2 and 3, respectively. The FAC densities (top row in Figure 1) for all three events show the typical dayside configuration associated with high-latitude duskside reconnection, with upward and downward FACs represented by red and blue colors, respectively. Only current densities above the 1σ confidence level are shown in the figure, and the 2σ threshold of the downward and upward FACs are indicated by solid and dashed lines, respectively. To adequately show the spatial distribution of current, a different maximum FAC density is used for each panel (see the color bars). The auroral images (bottom row in Figure 1) represent one-hour averages, which are obtained from ~30 snapshots taken approximately 2 minutes apart, and averaged after registering the images in magnetic latitude and local time. The FUV data are corrected for instrument background, ~500 counts, and dayglow emissions, ~4000 (~2000) counts in summer (spring and fall). The HiLDA emissions in these averages are only resolved from variations in the background auroral scene when the brightness exceeds ~800 R (500 counts). The uncertainty in the co-alignment of the auroral images is ±1 pixel ≈ 100 km ≈ 1° and is thus

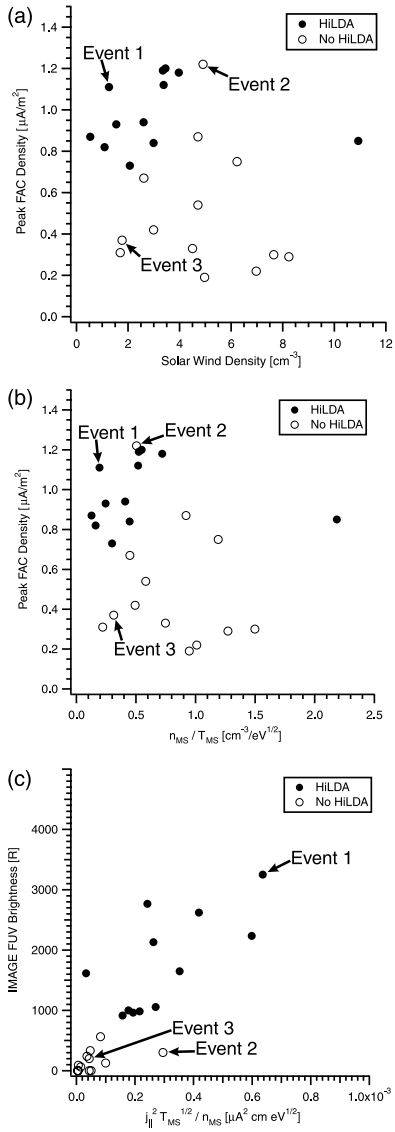

Figure 2. Analysis of 25 stable IMF intervals with IMF conditions typically observed during HiLDA event with respect to (a) peak FAC density and solar wind density, (b) peak FAC density and $n_{\rm ms}/\sqrt{T_{\rm ms}}$, and (c) auroral brightness and $j_\parallel^2\sqrt{T_{\rm ms}}/n_{\rm ms}$. Solid dots indicate the observation of HiLDA, while HiLDA was not measurable during events indicated with open dots.

lower than the 2° latitudinal resolution of the FAC maps attained from the Iridium observations. The 2σ confidence contours of the Iridium observations have been overlayed on the FUV averages.

[8] Event 1 shows typical HiLDA (bottom panel of Figure 1a), with bright emissions centered at 85° latitude in the afternoon sector. The peak upward FAC density observed during the one-hour interval in this region is 1.11 μA/m^2, the peak auroral brightness is 3251 R, and solar wind density averages 1.26 cm^{-3}. Comparison of the emissions with the 2σ upward FAC region (dashed contour) demonstrates good agreement in the location of both quantities. The FAC distribution during event 2 (Figure 1b) exhibits a configuration similar to the one observed during the previous event. However, the simultaneous auroral emissions associated with the upward FAC region peak at only 302 R. The peak FAC density is with 1.22 μA/m^2 comparable to the previous event, but the solar wind density is with 4.91 cm^{-3} almost four times as large as during event 1. Event 3 also does not show any auroral emissions above the HiLDA threshold associated with the Iridium upward FAC region. The peak brightness of 199 R during this event is below the lower limit of the color bar and therefore not shown in Figure 1c. The solar wind density of 1.77 cm^{-3} is comparable to event 1, while the peak FAC density of 0.37 μA/m^2 is a factor of 3 smaller.

[9] The analysis of all 25 stable IMF events with respect to the peak FAC density and the solar wind density is shown in Figure 2a, where solid dots indicate the presence of HiLDA in the high-latitude upward FAC region (12 events), while no auroral emissions are observed during events marked with open dots (13 events). From Figure 2a it is evident that the events form two clearly distinct distributions with respect to the occurrence of HiLDA, which are primarily observed during periods of low solar wind density (<4 cm^{-3}) and large FAC densities (>0.7 μA/m^2). That HiLDA tends to occur for low solar wind density is consistent with *Frey et al.* [2003]. The new result here is that upward currents are present for high solar wind densities without the occurrence of HiLDA. This demonstrates that it is more the aurora than the current systems which change.

4. Discussion

[10] Auroral emissions are induced when atoms or molecules excited by precipitating energetic particles relax to lower energetic states and emit photons of distinct wavelengths. The intensity of the aurora scales linearly with the energy flux of the precipitating population [e.g., *Carlson and Egeland*, 1995]. The IMAGE FUV observations of HiLDA show that this type of aurora is generated almost exclusively by precipitating electrons, while the proton contribution is negligible [*Frey et al.*, 2003]. For a current carried by electrons, the upward FAC density, $j_\parallel$, corresponds to an electron precipitation number flux, $J = j_\parallel/e$, where e is the electronic charge. For an auroral potential drop $\phi_\parallel$, the energy flux is approximately $\varepsilon \approx e\,J\,\phi_\parallel$ or $\varepsilon \approx j_\parallel\,\phi_\parallel$. The field-aligned potential drop is in turn governed by the current density and the thermal energy density of the precipitating population at high altitudes [*Knight*, 1973]. From the linearized Knight relation we have

$$j_\parallel = \frac{e^2\,n}{\sqrt{2\pi\,m\,E_{\rm th}}}\,\phi_\parallel, \tag{1}$$

where m is the electron mass, and n and $E_{\rm th}$ are the high-altitude density and thermal energy (temperature), respectively. We can then express the energy flux in terms of $j_\parallel$, $E_{\rm th}$, and n:

$$\varepsilon \propto \frac{j_\parallel^2\,\sqrt{E_{\rm th}}}{n}. \tag{2}$$

Since the auroral emission brightness is approximately proportional to ε, this shows that the ordering in Figure 2a is consistent with (2) if n is closely related to the solar wind

density. Equation (2) provides a physical basis for the ordering with solar wind density and suggests that $\sqrt{E_{th}}/n$ could also be used to organize the observations.

[11] To use equation (2), we first have to estimate n and E_{th}. The ordering of the auroral occurrence by the solar wind density suggests that the plasma on the high-altitude portion of the field lines, connected to the upward current region, is governed in large part by the solar wind and is therefore closely related to the magnetosheath plasma. We therefore estimate the magnetosheath density and temperature from the solar wind and IMF properties observed by ACE. Since the IMF conditions for all of these events correspond to quasi-perpendicular shocks, we use the jump conditions for a perpendicular fast-mode shock to estimate the sub-solar magnetosheath density and temperature from the ACE magnetic field and solar wind data. We assume that the density and temperature on the field lines of interest will approximately scale with the sub-solar magnetosheath values. The Mach number for these events is 4.8 on average with a range of 1.9 to 8.8. The magnetic field and density enhancement factors are 2.6 on average and range from 1.9 to 2.9. The magnetosheath densities, n_{ms}, and temperatures, T_{ms}, average 11 cm^{-3} and 295 eV and range from 1 to 30 cm^{-3} and 60 to 760 eV.

[12] There are large uncertainties in mapping the upward current regions to the magnetopause. A sophisticated calculation of n and E_{th} would need to use a magnetosheath hydrodynamic model and evaluate the density and temperature at the point on the magnetopause, where the field lines associated with either the HiLDA emissions or the upward currents map. However, as *Frey et al.* [2003] have found, the HiLDA events map close to the cusp implying that the mapping to the magnetopause suffers from large uncertainties. Moreover, we note that there are no magnetic field models, which properly include the intense DPY currents that are present during these conditions and which will significantly affect the mapping of the field lines in the current regions. We therefore regard an attempt to map the upward current field lines to the magnetopause as inherently unreliable and probably misleading. Nonetheless, the density and temperature on the field lines of interest should approximately scale with the sub-solar magnetosheath values. We therefore do not carry the estimate of n and E_{th} any further, but use the sub-solar magnetosheath values, n_{ms} and T_{ms}, as proxies. We note that n_{ms} is an upper limit for the actual density of the source precipitation population associated with HiLDA.

[13] Using the magnetosheath densities and temperatures estimated for each event, we plot the events in the same format as Figure 2a, but now plotting $j_{||}$ versus $n_{ms}/\sqrt{T_{ms}}$ (Figure 2b). The separation of cases with and without HiLDA remains essentially the same, with HiLDA occurring only for low values of $n_{ms}/\sqrt{T_{ms}}$ and high $j_{||}$. The one point without HiLDA that falls in the high $j_{||}$ low $n_{ms}/\sqrt{T_{ms}}$ range is event 2 (Figure 1b), in which HiLDA is not evident in the averaged FUV image, but in which individual images do show HiLDA. However, despite the outlier, the two distributions in Figures 2a and 2b are essentially the same, indicating that the density variation captures most of the dependence.

[14] To this point, we have treated the occurrence or absence of HiLDA in a binary fashion, whereas there are significant variations in auroral brightness between HiLDA events. For HiLDA events, the characteristic energy is typically 5 keV [*Frey et al.*, 2003], for which the deposited energy flux is $1.63 \cdot 10^{-3}$ $mW/m^2/R$ times the brightness. Figure 2c shows the auroral brightness versus $j_{||}^2\sqrt{T_{ms}}/n_{ms}$, where the HiLDA and no-HiLDA populations are clearly separated. Moreover, there is a significant positive correlation between brightness and $j_{||}^2\sqrt{T_{ms}}/n_{ms}$ (r = 0.83), confirming that equation (2) provides a reasonable framework for understanding the dependence of HiLDA occurrence and brightness on upstream conditions.

[15] The deposited energy flux can be estimated from the auroral brightness if one can also estimate the characteristic energy of the precipitating electrons. One could in principle refine the estimates for the characteristic energy somewhat for each event (to within a few keV) using the FUV data. But since we are using proxies for the right hand side of equation (2), in turn because the estimates of n and E_{th} are subject to the large uncertainties due to the intrinsic mapping difficulties near the cusp, a more exhaustive estimate of the energy flux from the multi-band FUV data was not justified. In any case, the error made by assuming a 5 keV energy is not much larger than the uncertainties in the refined characteristic energy estimates.

[16] The relationship denoted in equation (2) therefore organizes the occurrence and brightness of HiLDA in our statistical study. During event 1 (Figure 1a) the FAC density is quite large, while the particle density is particularly low. According to equation (2), these characteristics lead to a higher energy flux and thus represent favorable conditions for the observation of HiLDA, as shown in Figure 2b. On the other hand, the solar wind density during event 2 (Figure 1b) is much higher than the one observed during the first event, while the FAC densities are comparable in both events. The resulting lower energy flux (in comparison to event 1) induces significantly weaker auroral emissions that are not classified as HiLDA. Similarly, HiLDA is not observed during the third event (Figure 1c), because the low FAC density reduces the energy flux below the threshold, where auroral emissions can be generated efficiently.

5. Summary

[17] We have examined 25 stable IMF intervals with strong IMF B_y positive component for occurrence of high-latitude dayside aurora. Comparison with field-aligned currents from the Iridium constellation showed that HiLDA is predominantly observed when the quantity $j_{||}^2\sqrt{T_{ms}}/n_{ms}$, which is proportional to the energy flux, is large in the emission region. For intervals where HiLDA is not observed, the characteristic FAC structures are still present, but the energy flux associated with the upward currents is too low to produce considerable auroral emissions. This occurs when either the FAC density is too low, <0.7 $\mu A/m^2$, or when the solar wind density is too high, >4 cm^{-3}, or both. This dependence in occurrence and brightness of HiLDA is consistent with the Knight relation, provided that the plasma properties at high altitudes on field lines carrying the upward current are determined in large measure by the magnetosheath.

[18] **Acknowledgments.** We thank the ACE Team for use of the MAG and SWEPAM data made available via the ACE Level 2 Database.

References

Anderson, B. J., K. Takahashi, and B. A. Toth (2000), Sensing global Birkeland currents with Iridium engineering magnetometer data, *Geophys. Res. Lett.*, *27*, 4045–4048.

Burch, J. L. (2000), IMAGE mission overview, *Space Sci. Rev.*, *91*, 1–14.

Carlson, H. C., and A. Egeland (1995), The aurora and the auroral ionosphere, in *Introduction to Space Physics*, pp. 459–502, Cambridge Univ. Press, New York.

Frey, H. U., T. J. Immel, G. Lu, J. Bonnell, S. A. Fuselier, S. B. Mende, B. Hubert, N. Østgaard, and G. Le (2003), Properties of localized, high latitude, dayside aurora, *J. Geophys. Res.*, *108*(A4), 8008, doi:10.1029/2002JA009332.

Knight, S. (1973), Parallel electric fields, *Planet. Space Sci.*, *21*, 741–750.

McComas, D. J., S. J. Bame, P. L. Barker, W. C. Feldman, J. L. Phillips, P. Riley, and J. W. Griffee (1998), Solar Wind Electron Proton Alpha Monitor (SWEPAM) for the Advanced Composition Explorer, *Space Sci. Rev.*, *86*, 563–612.

Mende, S. B., et al. (2000a), Far ultraviolet imaging from the IMAGE spacecraft. 2. Wideband FUV imaging, *Space Sci. Rev.*, *91*, 271–285.

Mende, S. B., et al. (2000b), Far ultraviolet imaging from the IMAGE spacecraft. 1. System design, *Space Sci. Rev.*, *91*, 243–270.

Smith, C. W., J. L'Heureux, N. F. Ness, M. H. Acuña, L. F. Burlaga, and J. Scheifele (1998), The ACE magnetic fields experiment, *Space Sci. Rev.*, *86*, 613–632.

Waters, C. L., B. J. Anderson, and K. Liou (2001), Estimation of global field aligned currents using the Iridium system magnetometer data, *Geophys. Res. Lett.*, *28*, 2165–2168.

B. J. Anderson and H. Korth, Applied Physics Laboratory, Johns Hopkins University, 11100 Johns Hopkins Rd., Laurel, MD 20723, USA. (haje.korth@jhuapl.edu)

H. U. Frey, T. J. Immel, and S. B. Mende, Space Sciences Laboratory, University of California, Berkeley, Centennial Dr. at Grizzly Peak Blvd., Berkeley, CA 94720, USA.